

Fluorescence lifetime spectroscopy for guided therapy of brain tumors

Pramod V. Butte^a, Adam N. Mamelak^a, Miriam Nuno^a, Serguei I. Bannykh^b, Keith L. Black^a, Laura Marcu^{c,*}

^a Department of Neurosurgery, Cedars-Sinai Medical Center, Los Angeles, CA 90048, USA

^b Department of Pathology, Cedars-Sinai Medical Center, Los Angeles, CA 90048, USA

^c Biomedical Engineering, University of California, Davis, CA 95616, USA

ARTICLE INFO

Article history:

Received 14 September 2010

Revised 27 October 2010

Accepted 1 November 2010

Available online 3 November 2010

Keywords:

Glioma

Time-resolved fluorescence spectroscopy

In-vivo diagnosis

ABSTRACT

This study evaluates the potential of time-resolved laser induced fluorescence spectroscopy (TR-LIFS) as intra-operative tool for the delineation of brain tumor from normal brain. Forty two patients undergoing glioma (WHO grade I-IV) surgery were enrolled in this study. A TR-LIFS prototype apparatus (gated detection, fast digitizer) was used to induce in-vivo fluorescence using a pulsed N2 laser (337 nm excitation, 0.7 ns pulse width) and to record the time-resolved spectrum (360 – 550 nm range, 10 nm interval). The sites of TR-LIFS measurement were validated by conventional histopathology (H&E staining). Parameters derived from the TR-LIFS data including intensity values and time-resolved intensity decay features (average fluorescence lifetime and Laguerre coefficients values) were used for tissue characterization and classification. 71 areas of tumor and normal brain were analyzed. Several parameters allowed for the differentiation of distinct tissue types. For example, normal cortex (N = 35) and normal white matter (N = 12) exhibit a longer-lasting fluorescence emission at 390 nm ($\tau_{390} = 2.12 \pm 0.10$ ns) when compared with 460 nm ($\tau_{460} = 1.16 \pm 0.08$ ns). High grade glioma (grades III and IV) samples (N = 17) demonstrate emission peaks at 460 nm, with large variation at 390 nm while low grade glioma (I and II) samples (N = 7) demonstrated a peak fluorescence emission at 460 nm. A linear discriminant algorithm allowed for the classification of low-grade gliomas with 100% sensitivity and 98% specificity. High-grade glioma demonstrated a high degree of heterogeneity thus reducing the discrimination accuracy of these tumors to 47% sensitivity and 94% specificity. Current findings demonstrate that TR-LIFS holds the potential to diagnose brain tumors intra-operatively and to provide a valuable tool for aiding the neurosurgeon–neuropathologist team in to rapidly distinguish between tumor and normal brain during surgery.

© 2010 Elsevier Inc. All rights reserved.

Introduction

Gliomas represent 40% of all primary brain tumors, and treatment of gliomas poses a challenge due to their tendency to infiltrate the surrounding normal brain. The current 18-month survival rate of glioblastoma patients treated with surgery for biopsy only, partial resection, and complete resection ranges from 15% to 34%, making glioma one of the most lethal tumors (Brandes et al., 2008). There are multiple options available for treatment of gliomas. The most common is surgery followed by chemotherapy and radiation therapy (Ducray et al.; Fazekas, 1977; Robins et al., 2009). The extent of surgical resection is a primary determinant of outcome and extent of tumor resection is a single most important factor for longer survival (Berger, 1994; Byar et al., 1983; Sanai and Berger, 2008). Currently several techniques are employed by the surgeons to ensure near complete removal of the

tumor. These include stereotactic image-guided surgery based on pre-operative MRI scans and intra-operative magnetic resonance imaging (iMRI). iMRI provides real-time structural information concerning the extent of tumor and is used for defining the resection margins. The obvious advantage includes correction for the “shift” in the brain after craniotomy. However, the use of iMRI is scarce as the cost of such setup is high and requires specialized operating rooms including shielding and use of non-ferrous instrumentation. In addition, restriction in the patient positioning makes it difficult to operate on occipital and posterior fossa lesions. The actual pathological diagnosis can only be provided by biopsy and frozen section, which requires 15 to 20 minutes and can be used only in limited capacity. Even in the hands of most skilled surgeon, complete excision is limited by the tactile and visual feedback. Thus, in order to enhance the ability of surgeon to achieve a near completely excision of brain tumors without sacrificing the safety, new technologies are needed which can accurately distinguish between the tumor and normal brain and guide tumor resection in near-real time.

Laser-induced fluorescence spectroscopy (LIFS) represents a promising new adjunctive technique for in-vivo tissue diagnosis. Fluorescence spectroscopy involves exciting the endogenous fluorophores (label-free) within tissues and recording the emission. Earlier work has

* Corresponding author. Department of Biomedical Engineering, Genome Biomedical Science Facility, 451 Health Sciences Dr. Room 2513, University of California Davis, Davis, CA 95616, USA. Fax: +1 530 754 5739.

E-mail address: lmarcu@ucdavis.edu (L. Marcu).

demonstrated that steady-state LIFS of endogenous fluorophores (auto-fluorescence) has potential for diagnosis of neoplasms including brain cancer (Bottiroli et al., 1995; Bottiroli et al., 1998; Chung et al., 1997; Croce et al., 2003; Poon et al., 1992; Wagnieres et al., 1998). These include studies of glioblastoma (Butte et al., 2010; Croce et al., 2003; Lin et al., 2001; Marcu et al., 2004), astrocytoma (Lin et al., 2001), oligodendroglioma (Lin et al., 2001), and metastatic carcinoma (Lin et al., 2001). Fluorescence spectroscopy can be employed in two ways, steady-state or time-resolved fluorescence spectroscopy. The time-resolved measurement resolves fluorescence intensity decay in terms of lifetimes and thus provides additional information about the underlying dynamics of the fluorescence intensity decay. Time-resolved measurements are also independent of factors such as absorption by tissue endogenous fluorophores (e.g. blood), photobleaching or any other condition that may affect the fluorescence intensity. By measuring the fluorescence decay characteristics, which reflect the differences in the relaxation dynamics of distinct fluorescent molecules, time-resolved measurements have an ability to resolve overlapping spectra, and improve the specificity of the fluorescence measurement (Dickinson and Wehry, 1979; Lakowicz, 2006; Nithipatikom and McGown, 1987). Several groups including ours reported results on the utility of time-resolved LIFS (TR-LIFS) for diagnosis of tissue (Andersson-Engels et al., 1990; Cubeddu et al., 1995, 1989, 1992; Elson et al., 2004; Marcu et al., 2004; Siegel et al., 2003; Sud et al., 2006; Svensson et al., 2007; Vishwanath et al., 2002; Wagnieres et al., 1998). We reported the TR-LIFS of several types of brain tumors measured both ex-vivo in freshly excised tissue specimens (Butte et al., 2005; Marcu et al., 2004; Yong et al., 2006) and in-vivo in patients (Butte et al., 2010). Results from this work demonstrated the potential of the time-resolved fluorescence measurement to distinguishing brain tumors from uninvolved cerebral cortex and white matter and its increased specificity relative to steady-state fluorescence spectroscopy.

Based up on the knowledge derived from our latest study (Butte et al., 2010), a pilot work was conducted in a limited number of patients. The objective of this study was to determine the ability of TR-LIFS technique in discriminating glioma tumors (both high- and low-grade) from the surrounding normal brain tissue intra-operatively; and to evaluate challenges posed by intra-operative use of TR-LIFS. This work aims to establish the potential of TR-LIFS to enhance the ability of the neurosurgeon-neuropathologist team to rapidly distinguish between tumor and normal brain during surgery.

Materials and methods

Patient/samples

Forty two patients diagnosed with glioma were recruited for the study. The patients were scheduled for surgical removal of brain tumor and underwent the planned operation. During the procedure the TR-LIFS fiber optic probe was positioned above the areas of interest and the brain tissue was spectroscopically investigated ($N=186$). Areas with distinct pathologic features were selected based on the gross visual evaluation by the neurosurgeon that performed the surgery. Part of normal brain furthest from the visible tumor and tumor-free on neuro-navigational system was used to record the fluorescence emission of normal cortex, this ensured tumor free tissue. No biopsy was obtained from the normal brain tissues. Areas identified based on conventional diagnostic methods (e.g. pre-operative MRI) and surgeon experience as glioma tumors were TR-LIFS interrogated during the surgical resection. Fluorescence was measured from areas identified as tumor mass. To validate our results, intra-operative biopsy was conducted at each spectroscopically investigated spot, except at the areas not considered suitable for physical biopsy due to risks posed to patient. Tumor samples with relatively homogenous morphology were categorized as solid tumors, whereas infiltrated normal tissue at the boundary between the tumor

and normal brain tissue was categorized as margins. In this study, we present the data recorded from the solid tumors. The study was carried out with approval of the Cedars-Sinai Medical Center Institutional Review Board, with informed consent obtained from each patient.

Instrumentation

Experiments were conducted with an instrumental setup, which allowed for spectrally-resolved fluorescence lifetime measurements. The setup was similar with that used in our earlier pilot work (Butte et al., 2010). A schematic of the optical and electronic layout of the apparatus is shown in Fig. 1. Detailed account of this apparatus and its performance has been previously reported (Fang et al., 2004). Briefly, it consisted of a pulsed nitrogen laser (Lasertechnik Berlin, Berlin, Germany, model MNL200-ATM205, $\lambda = 337$ nm, pulse width = 700 ps FWHM) which was used as the excitation source, a custom made sterilizable bifurcated fiber-optic probe (CeramOptec, East Longmeadow, MA), an imaging spectrometer/monochromator (Chromex Inc., Albuquerque, NM, model 250is/sm, F/4.4, 600 gr/mm grating, blazed at 450 nm), a gated multi-channel plate photo-multiplier tube (MCP-PMT Hamamatsu, Bridgewater, NJ, model R5916-50, rise time = 180 ps) with a fast preamplifier (Hamamatsu, Bridgewater, NJ, model C5594, 1.5 GHz), a digital phosphor oscilloscope (TDS5104, Tektronix, Beaverton, OR, 5 Gsamples/s), and a computer workstation, and peripheral electronics. The instrument allowed for mobility as it was contained in a standard endoscopic cart ($70 \times 70 \times 150$ cm³) internally modified to accommodate the individual devices. To ensure a low noise levels from the electronics used such as a high voltage supply and preamplifier power supply, all the instruments were shielded from the main power supply using a medical grade Isolation transformer (Toroid® ISB-170A).

Delivery catheter

Light delivery and collection were implemented with a custom made bifurcated sterilizable probe. The probe consisted of non-solarizing silica/silica step index fibers of 0.11 numerical aperture (NA) (Fiberguide, New Jersey, NJ). It had a central excitation fiber of 600 μ m core diameter, surrounded by a collection ring of twelve 200 μ m core diameter fibers. The collection fibers were beveled at a 10° angle in order to improve excitation/collection overlap for small tissue-to-probe distances. The center-to-center separation between the excitation and collection fibers was 480 μ m. The probe was flexible throughout its entire length (3 meters) except of a 7 cm distal part consisted of a rigid stainless steel tube. This facilitated the mounting and micromanipulation of the probe. In contrast to previous study (Butte et al., 2010), a spacer with two slits on the opposite sides was added in front of the distal end of the probe. This allowed the probe to be in contact with the tissue while maintaining a fixed distance from the tissue. The two slits on the spacer enabled the surgeon to apply a suction tube to maintain a clear field. The laser light was coupled into the illumination channel of the probe with a standard SMA connector, while the distal end of the collection channel was formed into a straight line in order to facilitate coupling to the spectrograph. After tissue excitation, the emitted fluorescence light was collected and directed into the entrance slit of the spectrometer via the collection channel of the probe. A long-pass filter (WB360, Optima, Tokyo, Japan, $\lambda = 345$ nm) was placed before the entrance slit of the monochromator to prevent contamination of the fluorescence signal by the excitation light. The signal was then detected by the MCP-PMT, amplified by the fast preamplifier, and finally digitized at 8 bits resolution by the digital oscilloscope. The overall time resolution of the systems was approximately 300 ps. Based on the current design of the fiber optic probe and probe-to-tissue distance, the diameter of the tissue area excited during each measurement at the surface was ~1.2 mm, while the depth was related to the optical properties of the tissue. Based on the optical properties of human brain and tumor tissue (Yaroslavsky et al., 2002), we have

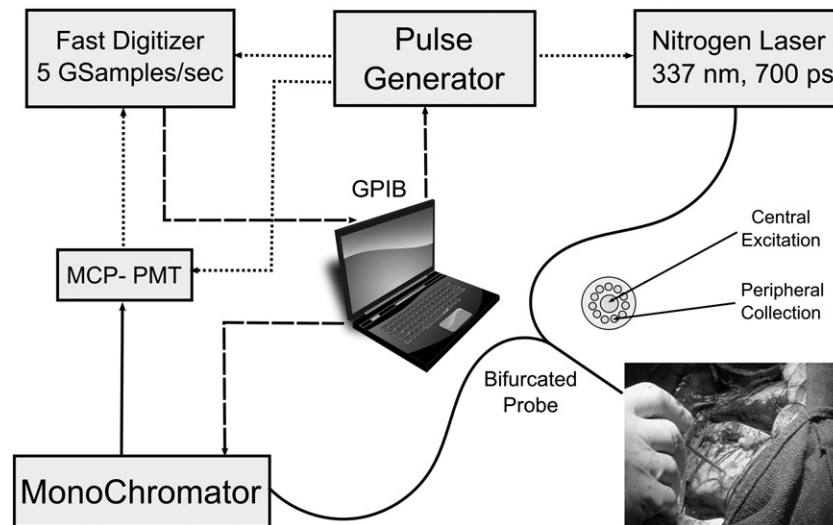


Fig. 1. Schematic of the TR-LIFS apparatus used in in-vivo study including the photo of the tip of the optical probe used on the brain tissue (cortex of a patient undergoing brain tumor surgery).

estimated the penetration depth of 337 nm between $\sim 250 \mu\text{m}$ and $400 \mu\text{m}$ for astrocytoma and normal cortex, respectively.

Experimental procedure

The fiber optic probe was positioned at 3 mm above the exposed brain tissue specimen with the help of a spacer to optimize the collection efficiency of the probe as previously reported (Papaioannou et al., 2004). The spacer also steadied the probe over the tissue, thus avoiding artifacts in the fluorescence emission due to pulsation of brain. Time-resolved emission of each sample was recorded in the 360–550 nm spectral range and scanned at 10 nm intervals. Five consecutive measurements of the fluorescence pulse emission at 390 and 460 nm were performed to assess the reproducibility of the fluorescence lifetime measurement. The energy output of the laser (at the tip of the fiber) for sample excitation was adjusted to $3.0 \mu\text{J}/\text{pulse}$. The area illuminated by the probe was 2.654 mm^2 , thus the total fluence per pulse received by the tissue was $1.39 \mu\text{J}/\text{mm}^2$, which was very well within the safety limits. After the spectroscopic analysis the tissue was biopsied at the exact site and sent for pathological investigation. Multiple data sets were obtained from areas considered normal and distant from the tumor area. Although no biopsy was performed on the normal tissues, all measured fluorescence emission data are presented.

Histopathological analysis

After a biopsy, each sample was fixed with 10% buffered formalin. Tissue samples were fixed on the slides and stained with H&E. All biopsy specimens were studied by the pathologist and correlated with fluorescence spectroscopy measurements. Histologically, gliomas were categorized as low grade: Oligodendroglioma, oligodendroastrocytoma, diffuse astrocytoma (WHO Grade II), intermediate grade: anaplastic astrocytoma (WHO grade III) and high grade: anaplastic oligodendroglioma, anaplastic oligoastrocytoma and glioblastoma multiforme (grades III–IV) based on the WHO grading (Louis et al., 2007). For the purpose of spectroscopic classification in this study, the gliomas were grouped as low grade glioma (LGG, grades I and II) and high grade glioma (HGG, grades III and IV).

TR-LIFS data analysis

In the context of TR-LIFS, the intrinsic fluorescence impulse response functions (IRF), $h(n)$, describes the real dynamics of the fluorescence decay. The IRF were recovered by numerical deconvolution of the measured input laser pulse from the measured fluorescence response transients. The Laguerre expansion technique (Jo et al.,

2004a,b, 2007) was used for deconvolution. Laguerre expansion technique was selected over the more conventional multi-exponential curve fitting for a set of reasons. It allows for faster deconvolution of the fluorescence IR. Since the Laguerre basis is orthonormal, it provides a unique and complete expansion of the decay function. This technique is also non-parametric thus does not require a priori assumption of the functional form of the decay. The deconvolution of fluorescence signal was performed using four Laguerre coefficients. Consequently, this allows for the approximation of fluorescence systems with unknown and complex relaxation dynamics such as that of biological tissues. This method allows a direct recovery of the intrinsic properties of a dynamic system from the experimental input-output data. The technique uses the orthonormal Laguerre functions $l_n^q(n)$ to expand the IRF and to estimate the Laguerre expansion coefficients (LEC). The fluorescence decay profile describes the biochemical and morphological characteristics of the tissue. Each Laguerre coefficient describes various dynamics of a complex fluorescence decay curve, i.e. lower order functions describe slower decay characteristics and higher order Laguerre functions describe the faster decay characteristics. The coefficients of the Laguerre function describe the relative contribution of each Laguerre function to the observed fluorescence decay. In order to characterize and model complete temporal dynamics, all the Laguerre coefficients were computed and used as parameters along with the average lifetime which indicates a single value on a complex fluorescence decay curve.

Parameters selection. Once the fluorescence IRFs were estimated for each emission wavelength, the steady-state spectrum (I_2), was computed by integrating each intensity decay curve as a function of time. In order to derive parameters from the intensity values, normalized fluorescence spectra was obtained by dividing the discrete intensities values with the intensity value at the peak emission. It has been shown that blood absorption affects all the wavelengths equally and using intensity ratios negated the requirement for spectral correction (Andersson-Engels et al., 1990). Thus, instead of using normalized intensity values, we have used the intensity ratios, which only describe the relative intensity between various spectral bands. The wavelengths around the peak emission bands ($I_{380}, I_{390}, I_{440}, I_{450}, I_{460}, I_{470}$) and the wavelengths around the lowest fluorescence emission intensity ($I_{370}, I_{480}, I_{490}, I_{500}, I_{510}, I_{540}, I_{550}$) were selected for computing the intensity ratio, using all the permutations. Further, to characterize the temporal dynamics of the fluorescence decay, two sets of parameters were used: (1) the average lifetime (τ_f) computed as the interpolated time at which the IRF

decays to $1/e$ of its maximum value; and 2) the normalized value of the corresponding LECs. Thus, a complete description of fluorescence from each sample as a function of emission wavelength, λ_E , was given by the variation of a set of spectroscopic parameters at distinct wavelengths (emission intensity— I_λ , average lifetime of fluorescence emission— τ_f , and Laguerre coefficients LEC $_f$). The parameters which were derived from the fluorescence data were $I_{390/440}$, $\tau_{380/440}$, $\tau_{390/440}$, $I_{390/450}$, $I_{390/460}$, $I_{380/370}$, $I_{440/550}$, $I_{390/370}$, $I_{440/370}$, $I_{450/370}$, $I_{460/370}$, $I_{470/370}$, $I_{480/370}$, $I_{380/550}$, $I_{390/550}$, $I_{440/550}$, $I_{450/550}$, $I_{460/550}$, $I_{470/550}$, $I_{480/550}$, τ_{370} , τ_{380} , τ_{390} , τ_{440} , τ_{450} , τ_{460} , τ_{470} , τ_{480} , $I_{380/370}$, $I_{380/400}$, $I_{380/440}$, $I_{380/450}$, $I_{380/460}$, $I_{380/470}$, $I_{380/480}$, $I_{380/490}$, $I_{380/500}$, $I_{380/510}$, $I_{380/520}$, $I_{380/530}$, $I_{380/540}$, $I_{390/400}$, $I_{390/440}$, $I_{390/470}$, $I_{390/480}$, $I_{390/490}$, $I_{390/500}$, $I_{390/510}$, $I_{390/520}$, $I_{390/530}$, $I_{390/540}$, $I_{440/380}$, $I_{440/390}$, $I_{440/400}$, $I_{440/450}$, $I_{440/460}$, $I_{440/470}$, $I_{440/480}$, $I_{440/490}$, $I_{440/500}$, $I_{440/510}$, $I_{440/520}$, $I_{440/530}$, $I_{440/540}$, LEC-1 $_{380}$, LEC-1 $_{390}$, LEC-1 $_{440}$, LEC-1 $_{450}$, LEC-1 $_{460}$, LEC-1 $_{470}$, LEC-1 $_{480}$, LEC-1 $_{490}$. This analytical approach for characterization of fluorescence decay was recently developed by our research group and described in detail elsewhere (Jo et al., 2005).

Data reduction and statistical analysis. To identify a set of spectroscopic parameters from the list above that best discriminate between various tissue types, a univariate statistical analysis (one-way ANOVA) was used to compare the spectroscopic parameters (I_λ , τ_f , and LECs) at every λ_E for each type of tissue defined by histology. A p -value of <0.05 was assumed to indicate statistical significance. First, a systematic comparison of the p -values obtained for each parameter at every λ_E allowed to identify a set of spectroscopic parameters (I_λ , τ_f , and LECs at specific λ_E 's yielding the lowest p -values) likely to provide means of discrimination among different brain tissue types. Parameters were tested for statistical significance amongst various combinations of two tissue types. Significant parameters were grouped into six separate sets based on their ability to discriminate between these two types. All statistical analysis was conducted using MATLAB® (Mathworks Inc.). Second, as these parameters were incorporated in linear discriminant analysis, Lilliefors test was performed to ensure the parameters included in the classification were normally distributed. Although, discarding the parameters based on their non-normality reduced the number of parameters and introduced a confounding factor, using non-normal parameters with linear discriminant functions analysis can lead to misclassification (Baron, 1991; Bello, 1992; Rausch and Kelley, 2009). The final parameters which satisfied the selection criteria and were included in classification scheme are listed in Table 1.

Classification

In order to classify and predict the fluorescence signal acquired we have adopted a classification algorithm based on the binary separation of tissue types using linear discriminant function analysis (DFA). This approach is a novel application designed to identify a unique tissue sample intra-operatively in near real-time (Fig. 2).

Training phase. Fluorescence emission data was divided in four groups (NC, NWM, LGG and HGG). Since no specific parameter was found to

Table 1
Main sets of fluorescence parameters use in brain tissue classification (NC, NWM, LGG, HGG).

Sets	Parameters used for classification
NC vs. NWM	τ_{440} , τ_{460} , LEC-0 $_{450}$, LEC-0 $_{60}$, $\text{avg}(I_{440} + 450 + 460)/\text{avg}(I_{380} + 390)$, I_{370}/I_{390}
NC vs. LGG	I_{440}/I_{550} , I_{460}/I_{550} , LEC-1 $_{390}$, LEC-1 $_{440}$, LEC-1 $_{540}$, LEC-1 $_{370}$
NC vs. HGG	$\text{avg}(I_{540} + 550) / \text{avg}(I_{440} + 450 + 460)$, I_{370}/I_{380} , I_{540}/I_{440} , I_{450}/I_{550} , I_{460}/I_{540} , τ_{380} , LEC-1 $_{390}$
NWM vs. LGG	$\text{Avg}(\tau_{440} + 450 + 460) / \text{avg}(\tau_{540} + 550)$, I_{440}/I_{380} , I_{550}/I_{380} , I_{440}/I_{370} , LEC-0 $_{460}$, τ_{550} , LEC-0 $_{460}$, LEC-0 $_{550}$
NWM vs. HGG	I_{390}/I_{440} , I_{460}/I_{390} , LEC-0 $_{550}$, LEC-1 $_{450}$
LGG vs. HGG	$\text{Avg}(\tau_{380} + 390) / \text{Avg}(\tau_{440} + 450 + 460)$, I_{440}/I_{370} , I_{440}/I_{370} , I_{450}/I_{370} , I_{460}/I_{450} , I_{460}/I_{370}

be useful in discriminating all tissues types, the discriminant model was divided in six sub-models of binary sets which classify all the data into specific tissue types (normal NC vs. LGG or , NC vs. HGG or, LGG vs. HGG, etc.). Parameters were selected independently for each tissue sub-group categorized. A one-way ANOVA was used to compare parameters for each tissue group, thereby identifying the parameters that best discriminate between the different tissue types. In order to test for normal distribution, Lilliefors test was performed and the parameters with non-normal distribution were discarded. Once the parameters for each set of classifying models were determined, DFA coefficients were calculated and the value of the centroid noted.

Test phase. A step-wise linear discriminant analysis was used to classify tumor tissue (NC, NW, LGG, and HGG) into two tissue sub-group models (e.g. NC versus NWM) according to a set of tissue characteristics (parameters) that were derived a-priory during the training phase. In general, this approach determines which variables (parameters) account for most of the differences in the mean profile of the groups being compared. For instance, the larger the difference between the means of two tissue types relative to the variability within each tissue group, the better the discrimination between the two groups.

The classification criterion aims to assign a tissue sample to the group with the highest conditional probability (e.g. Baye's Rule) while minimizing classification error. For instance, consider two groups, Baye's rule assigns tissue as belonging to group 1 whenever $P(G_1|x) > P(G_2|x)$. In general, we are interested in the probability $P(G_i|x)$ that a tissue type belongs to group i , given a set of measurements x . Applying Baye's Theorem yields the following posterior distribution:

$$P(G_i|x) = p(x|G_i)P(G_i),$$

where $p(x|G_i)$ describes the probability of getting a particular set of measurement x given that the tissue comes from group i . $P(G_i)$ is the prior probability for group i before data on measurements x is taken into account. Equal prior probability were assumed for all tissue types. The posterior distribution was used to determine group membership for all six two-group tissues being compared. The total number of posterior probabilities obtained from these models for each tissue type was $n - 1$, where n was the number of tissue types being evaluated. The posterior probabilities were then averaged as shown in Fig. 2 and compared in order to determine the group to which the sample belongs to.

In order to eliminate bias in sensitivity and specificity due to data driven predictions, a leave-one-out cross validation approach was used to calculate the classification (discriminant) score and thereby predict group membership. In the leave-one-out cross-validation, a single set of spectroscopic data was removed from the study population and used in the validation process. The cutoff value was evaluated in a data-driven way from the remaining $n - 1$ parameters. Thereafter, the resulting cutoff value was applied to the newly acquired data. This tissue was then classified as a true positive, a false positive, a false negative, or a true negative, depending on whether or not this tissue was classified as belonging or not to the group membership being assessed. This process was repeated for all parameters in the dataset, and the results based on all of the parameters were then used to evaluate the sensitivity and specificity corresponding to the cutoff value that was derived in the $n - 1$ parameters.

Results

Although we have collected fluorescence emission data from a large number of samples ($N = 186$), Histopathological information on all the samples was not available on discretion of surgeon due to various factors such as proximity to functional area, lack of specificity in localizing the exact volume of biopsied tissue excited using laser. Based on the availability of biopsy specimens, we only report the

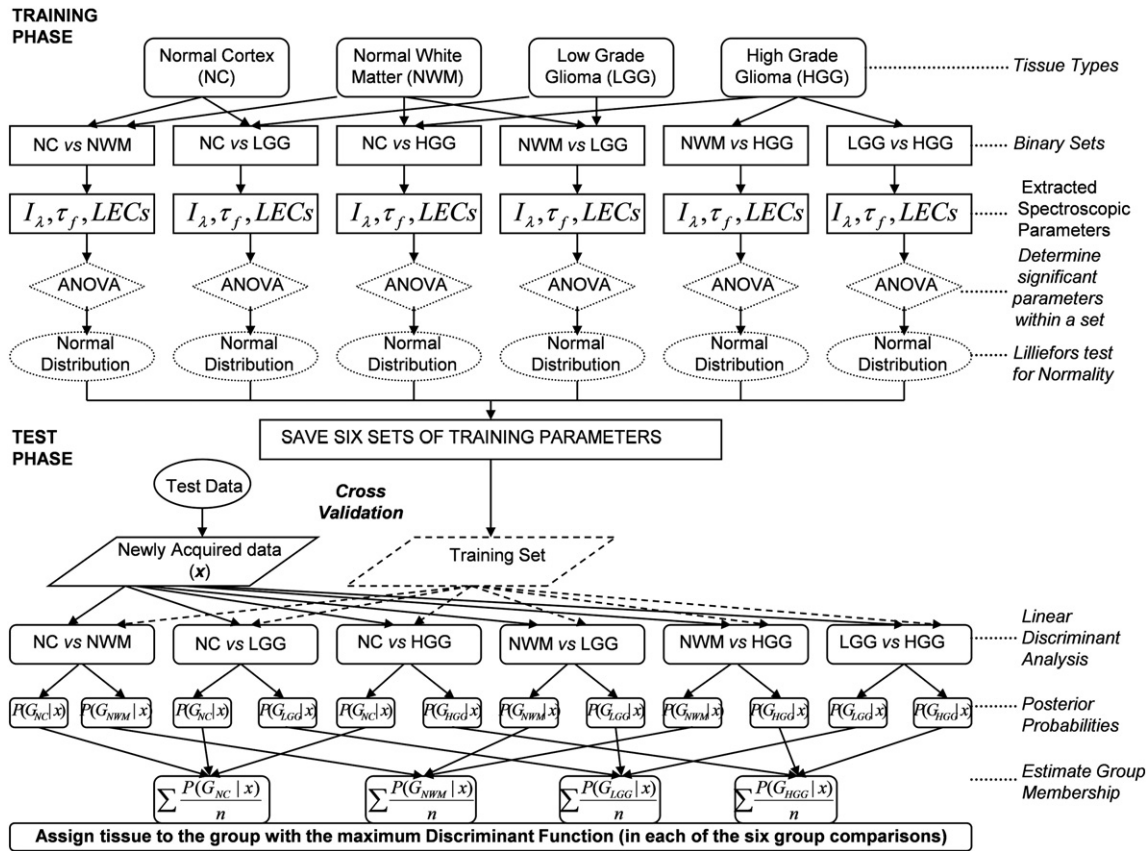


Fig. 2. Flowchart illustrating the classification algorithm to identify a single sample time-resolved fluorescence spectroscopy data acquired intra-operatively. The linear discriminant analysis provides posterior probabilities of the sample belonging to the groups being analyzed. The average probability is calculated for each type of tissue by using all the posterior probabilities.

results on 71 individual regions of measurement correlated with histopathology (tumor areas) and MRI data (normal cortex areas). These included normal cortex ($N=35$); normal white matter ($N=12$); low grade glioma ($N=7$) including mixed oligoastrocytoma and oligodendroglioma ($N=4$) and diffuse astrocytoma ($N=3$); high grade glioma ($N=17$) which include glioblastoma ($N=11$), anaplastic oligodendroglioma ($N=5$) and one recurrent glioma with radiation necrosis ($N=1$). Recurrent glioma with radiation necrosis was included in the study as there was no evidence of scar tissue with fibrosis which altered fluorescence characteristics due to presence of collagen. Representative feature of the tissue histopathology are given in Fig. 3A and B.

Time-resolved fluorescence characteristics

All samples (Fig. 3C and D) showed relatively broad emission spectrum with a varying degree of reduced emission at 415 nm which corresponds to the Soret band of hemoglobin absorption (Beychok et al., 1967). This variability of the signal at 415 nm was due to different blood amounts interfering with optical probe during the surgery. The average signal-to-noise ratio (SNR) obtained was around 40 dB, it ranged from 2.5 dB at the lowest and 60 dB at the peak emission. The τ_f values followed a similar trend for all tissue types; lifetime at blue-shifted wavelengths (~ 390 nm) was typically longer when compared with red-shifted wavelengths (>440 nm). LECs as a function of wavelengths provided additional information to fluorescence spectra and lifetime for comparing and classifying tissue samples. The zeroth-order coefficient (LEC-0) and the first order (LEC-1) were used to classify the tissues. LEC-0 closely followed the average lifetime in data, whereas LEC-1 provided information regarding faster dynamics in the fluores-

cence decay curve and thus was used as additional parameters for tissue characterization.

Normal cortex (NC)

NC fluorescence was characterized by a broad fluorescence emission with two distinct peaks centered at 390 and 440 nm (Fig. 3C and D), with the emission slightly higher at 440 nm when compared with 390 nm. The τ_f values at 390 nm ($\tau_{390} = 2.12 \pm 0.10$ ns) were longer than those at 440 nm ($\tau_{460} = 1.16 \pm 0.08$ ns). The LEC-1 values at 390 nm ($LEC-1_{390} = -0.032 \pm 0.019$) were lower when compared with LEC-1 values at 440 nm ($LEC-1_{440} = 0.095 \pm 0.010$), a trend that mirrored the τ_f values.

Normal white matter (NWM)

The NWM spectra (Fig. 3C and D) showed a main peak emission shifted to 450 nm when compared to NC. The emission at 390 nm ($I_{390} = 0.63 \pm 0.07$) was also lower when compared to NC. The average lifetimes at 390 nm ($\tau_{390} = 1.933 \pm 0.15$ ns) and 440 nm ($\tau_{440} = 1.193 \pm 0.11$ ns) were similar to those of NC. The LEC-0 had similar values at 390 nm ($LEC-0_{390} = 0.766 \pm 0.02$) and 440 nm ($LEC-0_{440} = 0.7269 \pm 0.018$) to those on NC. The LEC-1 at 390 nm ($LEC-1_{390} = -0.00885 \pm 0.002$) were also similar to LGG while at 440 nm ($LEC-1_{440} = 0.105 \pm 0.020$) was similar to NC.

Low grade glioma (LGG)

The LGG demonstrated a main peak emission centered at 440–450 nm. A secondary peak was present around 390 nm, however, this was lower ($\sim 30\%$) when compared with the main peak emission

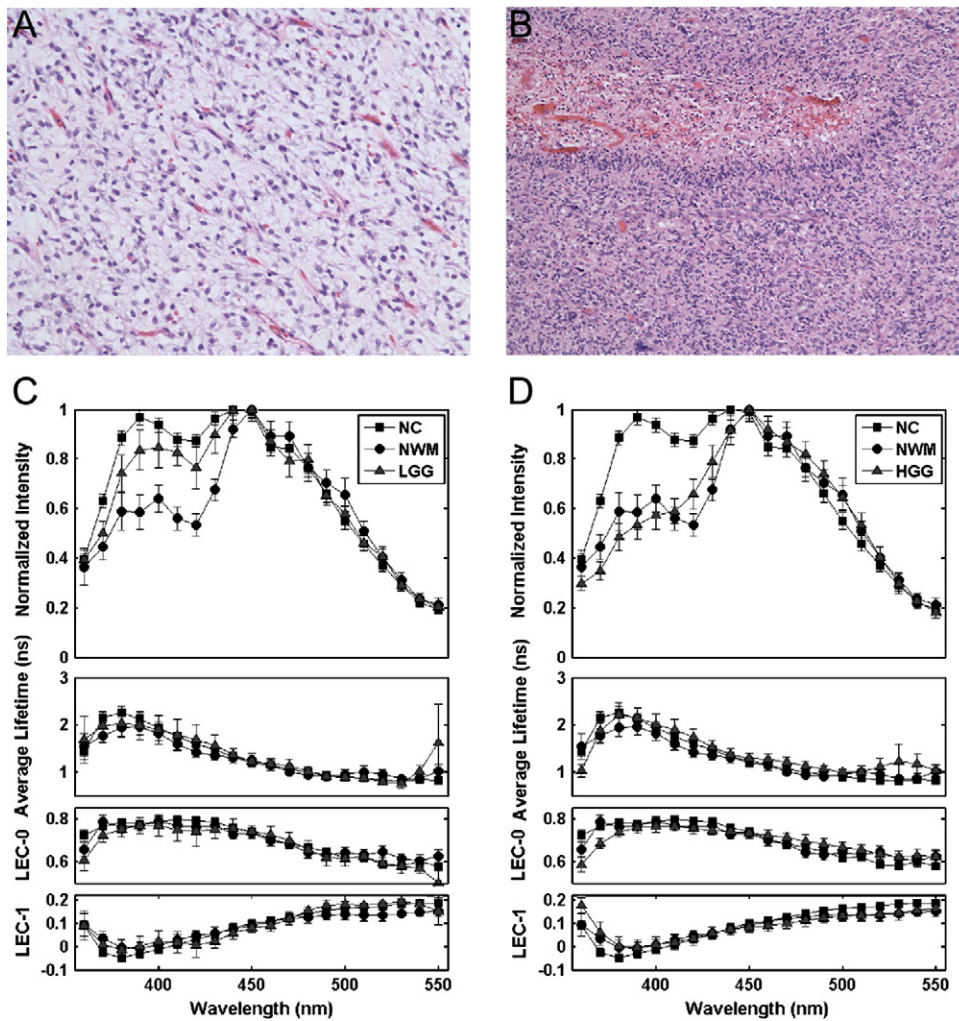


Fig. 3. Slides representing a typical H-E staining histopathology (magnification: 200 \times) from the sample of (A) LGG section illustrates moderately cellular proliferation of slightly enlarged atypical nuclei infiltrating through the white matter, (B) HGG sections show densely cellular proliferation of atypical cells associated with numerous mitoses and endothelial proliferation. Comparison of average fluorescence values mean \pm SE of the spectroscopic parameters, emission spectra intensity, average lifetime, average Laguerre coefficients (LEC-0, LEC-1) across the emission wavelengths for distinct brain tissue types (C) normal cortex, normal white matter and high grade glioma, (D) normal cortex, normal white matter and low grade glioma.

(Fig. 3C). The τ_f values appeared slightly longer than those observed in NC, both at 390 nm ($\tau_{390} = 1.81 \pm 0.35$ ns) and 440 nm ($\tau_{440} = 1.38 \pm 0.31$) but this difference was not found statistically different. The LEC-0 at 390 nm ($LEC_{0390} = 0.7749 \pm 0.34$) was similar to 440 nm ($LEC_{0440} = 0.775 \pm 0.33$). The LEC-1 at 390 nm was ($LEC_{1390} = -0.0077 \pm 0.0045$), and LEC-1 values observed at 440 were lowest in ($LEC_{1440} = -0.068 \pm 0.0041$) compared to other types of tissues. Notably, we determine differences within the sub-sets of LGG (Fig. 4A). The emission of diffuse astrocytoma was found different than that of oligoastrocytoma and oligodendroglioma. This tumor type have a higher emission intensity and longer τ_f at 390 nm compared with oligodendroglioma. When the fluorescence from oligoastrocytoma and oligodendroglioma is studied separately, the τ_f at 390 nm was shorter ($\tau_{390} = 1.57 \pm 0.2$ ns) compared with diffuse astrocytoma ($\tau_{390} = 2.58 \pm 0.5$ ns).

High grade glioma (HGG)

The HGG demonstrated a main peak emission centered at 450 nm. A secondary peak was present around 390 nm. This was lower (~40%) when compared with 450 nm emission (Fig. 3D). Average lifetime observed at 390 nm ($\tau_{390} = 1.93 \pm 0.18$ ns) was longer than at 440 nm ($\tau_{440} = 1.138 \pm 0.12$ ns). The LEC-0 at 390 nm ($LEC_{0390} = 0.761 \pm 0.023$) was higher than at 440 nm ($LEC_{0440} = 0.0394 \pm 0.016$). The values of the

LEC-1 observed at 390 nm and 440 nm were $LEC_{1390} = -0.0183 \pm 0.34$, ($LEC_{1440} = 0.0875 \pm 0.0223$, respectively. As observed in LGG tumors, HGG demonstrated variation in the fluorescence emission characteristics based on histopathological sub-classification. It was noted that the fluorescence emission data collected from HGG demonstrated a great degree of variability. Glioblastoma multiforme (GBM) fluorescence emission characteristics were similar to low-grade oligodendroglioma with a shorter τ_f at 390 nm ($\tau_{390} = 2.145 \pm 0.25$ ns) compared to anaplastic oligodendroglioma ($\tau_{390} = 2.66 \pm 0.5$ ns) with longer τ_f at 390 nm. A single sample of recurrent glioma with necrotic changes was characterized by a single emission peak at 390 nm of wavelength and overall faster average lifetime ($\tau_{390} = 1.11$ ns, Fig. 4B). In addition, changes were observed for fluorescence parameters between the samples obtained from the HGG core and the margins of the tumor, within the same patient (data not shown). The fluorescence parameters retrieved for the measurement within the tumor margins resembled those of LGG.

Statistical analysis and classification

Table 1 summarizes six main sets of fluorescence parameters able to discriminate between two tissue types as identified using ANOVA test. Table 2 depicts the classification results using both spectral intensities ratios and time-resolved parameters; and computed based on the

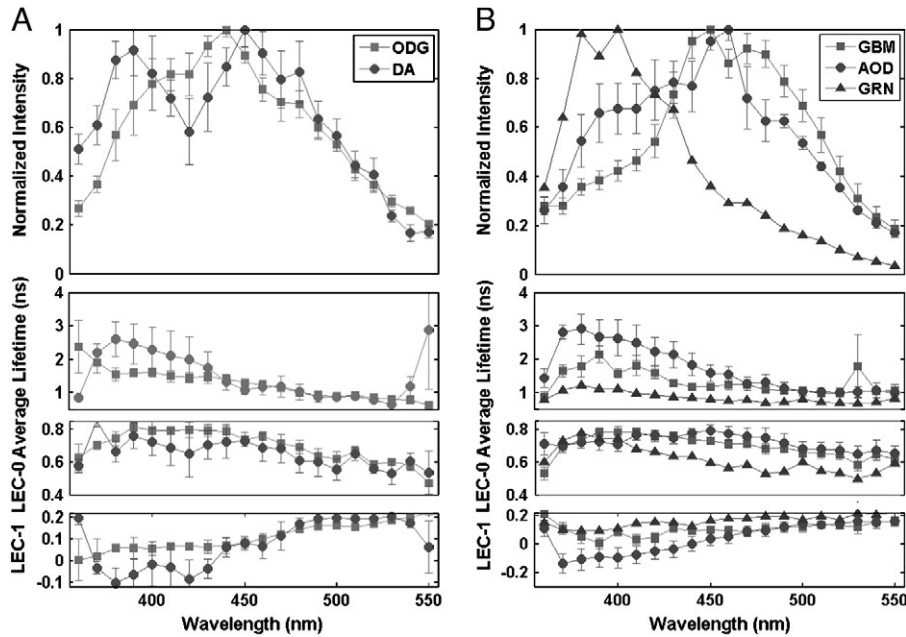


Fig. 4. Comparison of fluorescence values mean \pm SE of spectroscopic parameters, emission spectra intensity, average lifetime, and average Laguerre coefficients (LEC-0, LEC-1) across the emission wavelengths to demonstrated the variation of these parameter as a function of glioma sub-types. (A) Low grade gliomas: oligodendroglioma and oligodendroastrocytomas group together (ODG) show a faster average lifetime at 390 nm when compared with diffuse astrocytoma (DA); and (B) high grade gliomas; Glioblastoma multiforme (GBM), anaplastic oligodendroglioma (AOD) and recurrent glioma with radiation necrosis (GRN). AOD demonstrate a longer average lifetime at 390 nm when compared with GBM. The fluorescence intensity at 440–460 nm from GRN with necrosis was lower when compared with 390 nm due to lower NADH/NAD(P)H levels in the necrotic tissue and presence of collagen. Although DA were classified as LGG, the fluorescence emissions signature matches closely that of AOD.

algorithm that allows for binary separation of distinct tissue groups using LDA. LGG were separate with very high sensitivity (100%) and specificity (98%). All LGG were correctly identified, except for one measurement when NC was classified as LGG. The classification accuracy dropped when classifying the HGG to sensitivity of 47% and specificity of 95%. We attribute this low sensitivity value for HGG to high variability in the fluorescence signature of HGG. Table 3 depicts the classification results while using only the spectral intensity ratios. The classification results depicted in Table 3 (classification based on only spectral intensity ratios) and Table 2 (classification based on both spectral intensity ratios and time-resolved parameters) showed that the addition of time-resolved parameters improves primarily the sensitivity for indentifying NC, NWM and HGG; however, the specificity remains relatively similar for the two classifications approaches.

Discussion

This study demonstrates that TR-LIFS can accurately differentiate LGG from normal tissues (100% sensitivity and 98% specificity). These finding are in agreement to those reported previously by our group (Butte et al., 2010). Differentiating between LGG and NWM is critical when aiming to achieve a complete excision at the margins, as the tumor is likely to be surrounded by NWM. Detection of LGG represents a major challenge to current tumor resection since LGG lack the vascularity of HGG and are often visually bland. As such they are far more difficult to

differentiate from surrounding normal brain than HGG. Further, these tumors typically infiltrate into surrounding tissues that maintain function, often resulting in surgeons performing only biopsies or limited resections. Several recent studies have demonstrated that the extent of resection of LGG correlates with long term survival and the potential for cure (Sanai and Berger, 2008; Smith et al., 2008). These findings are especially important in light of the fact that these tumors are more prevalent in younger patients, for whom increased life expectancy and cure is highly desirable. Consequently, one of the great potential applications of TR-LIFS is the ability to differentiate LGG from normal brain. As such, it may prove to be an extremely useful adjunct to increasing the extent of resection in LGG surgery.

The HGG were classified with high specificity (94%) that would indicate minimum false positive results. Our results, however, demonstrate that current test have very low sensitivity (47%) in classifying this broad tumor type. We attribute this to the high variability in the TR-LIFS signals obtained from various subclasses HGG (Fig. 4B). We also found that these tumors are highly heterogeneous in terms of their fluorescence spectroscopic features. Such differences may also be attributed to the large variance in the protein expression (Umesh et al., 2009) within the same HGG tumor. Generally, HGG cells are more pleomorphic when compared with LGG. Thus, an important aspect to be investigated in future studies is to determine how well heterogeneities in HGG can be distinguished using TR-LIFS derived parameters.

Table 2
Classification results using both temporal and spectral parameters: sensitivity (SE) and specificity (SP) in the discrimination of NC, NWM, LGG, and HGG.

	Fluorescence spectroscopy				Sensitivity (%)	Specificity (%)
	NC	NWM	LGG	HGG		
NC (n = 35)	27	3	1	3	79.41%	78.26%
NWM (n = 12)	4	8	0	0	66.67%	90.63%
LGG (n = 7)	0	0	7	0	100.00%	98.44%
HGG (n = 17)	6	3	0	8	47.06%	94.64%

Table 3
Classification results using on the spectral parameters: sensitivity (SE) and specificity (SP) in the discrimination of NC, NWM, LGG, and HGG.

	Fluorescence spectroscopy				Sensitivity (%)	Specificity (%)
	NC	NWM	LGG	HGG		
NC (n = 35)	24	4	2	3	72.73%	81.40%
NWM (n = 12)	2	3	4	3	25.00%	87.50%
LGG (n = 7)	0	0	7	0	100.00%	96.83%
HGG (n = 17)	6	4	2	4	25.00%	94.55%

We anticipate that a more comprehensive classification based on the biochemical information and immuno-histochemistry, rather than structural features (H&E staining) will help in classifying the HGG with higher accuracy. Due to small sample size available for this study, we grouped all the HGG samples together. Such grouping of multiple subclasses (pro-neural, astral, etc) most likely contributed to the low sensitivity values. In order to obtain an unbiased estimation of the classification accuracy, a larger set of data needs to be obtained and the training set and the test set used have to be completely independent. Consequently, a higher number of HGG need to be investigated along with the biochemical heterogeneities within the same tumor for a more comprehensive assessment of the ability of TR-LIFS to distinguish HGG tissue from normal brain tissue and in particular to improve the sensitivity of the measurement.

When compared with our previous study, the fluorescence characteristics closely matched with the exception of average lifetime values at 390 nm in LGG and NC areas. The NC measurements were obtained from a clear area which is further from the tumor site and confirmed “tumor free” with the help of neuronavigational MRI images and neurosurgeon experience. Normal cortex tissue is covered with layers of arachnoid and pia mater which consists of collagen fibers. Collagen has peak fluorescence at 390 nm of wavelength with an average lifetime of ~3 ns (Marcu et al., 2001). The variation in collagen type and amount between optical probe and the actual brain tissue may have contributed to the variation in the averaged lifetime values. Due to our inability to perform a biopsy on the normal healthy brain, we were unable to confirm this hypothesis. We note that the average lifetime values at 390 nm (1.45 ± 0.4 ns) of LGG in our previous study (Butte et al., 2010) were found shorter than those observed in the current study (1.58 ± 0.2 ns). To understand this difference in average lifetime value at 390 nm from LGG samples, we sub-divided the LGG tumors in mixed astrocytoma, oligodendroglioma and diffuse astrocytomas. It was observed that the oligodendral tumors had shorter / faster lifetime at 390 nm compared to tumors of astrocytic origin such as diffuse astrocytomas (Fig. 4A). The five samples in our previous study were from mixed oligoastrocytoma ($N=3$) and oligodendroglioma ($N=2$) which account for faster average lifetimes at 390 nm. In the current study, the average lifetime at 390 nm is longer due to additional four samples of diffuse astrocytomas, which has a longer lifetime at 390 nm as seen in Fig. 4A, grouped with oligodendral tumors. This is a significant finding as the diffuse astrocytomas have a tendency to turn malignant in to GBM. The difference in average fluorescence lifetime at 390 nm observed during surgical resection can be used as an indicator to change the type of resection. We hypothesize that this difference may be attributed to the IDH-1 mutation in oligodendral tumors (Hartmann et al., 2009; Yan et al., 2009), which affects the NADP⁺-dependant isocitrate dehydrogenase leading to an increase in 2-hydroxyglutarate and α -ketoglutarate in the cells. α -ketoglutarate is in equilibrium with glutamate, and excess of glutamate may lead to an up-regulation of glutamate decarboxylase (GAD) which has peak fluorescence emission at 390 nm of wavelength and average lifetime of 1.8–2.1 ns (Rosato et al., 1989). We are in the process of designing new experiments to confirm presence of both collagen and Glutamate decarboxylase as the fluorophores responsible for this variation.

The classification using only the spectral intensity ratios demonstrated a significant drop in the sensitivity and specificity of normal white matter and high grade glioma, whereas, time-resolved fluorescence data without any correction for spectral response yielded superior accuracy. This emphasizes the potential of using additional time resolved fluorescence in the intra-operative setting in which factors which affect the spectral intensity values such as hydration, temperature, and absorption by blood cannot be controlled. The fluorescence decay characteristics are immune to factors noted above and thus can be more robust in characterizing tissues intra-operatively. Secondly, a high specificity also signifies the reduced risk of resecting viable normal brain. With the time-resolved data the sensitivity of detecting

tumor increased which would allow the surgeon to perform a more aggressive resection with low morbidity associated surgical resection.

Limitations of classification method

While we were able to acquire large fluorescence data set, we could not include all the data in the classification stage. We were limited by constraints on the number of biopsies performed on the brain tissue. Only a limited number of spectroscopic data sets can be correlated with the histopathological diagnosis. Consequently, we use a cross-validation method (leave-one-out) to test our algorithm. Although cross-validation method can remove the bias in such analysis, there is a danger in overestimation of the data by selecting the best possible outcome. In addition, we used known outcome to determine the best set of parameters to be used in the classification. Such assumption in the analysis can lead to distorted and predetermined results (Kriegeskorte et al., 2009). In order to avoid this issue we anticipate acquiring more data with histopathological analysis in the future in order to have a separate training set and the test set. Furthermore, we want to select the wavelengths used in analysis based on the physical relevance to avoid the bias in selection of parameters.

In-vivo measurements, challenges and opportunities for glioma diagnosis

The validation and ultimately the use of TR-LIFS for clinical diagnostics would have to account for a number of challenges related to various factors including the biological diversity of the brain tumors, ability to validate the spectroscopic technology against local pathophysiological transformation in brain tissue, and label-free fluorescence-based technology to operate in clinical environment.

(A) Brain tumors are characterized by a broad biochemical, molecular, and metabolic diversity. Consequently, these tumors are likely to have a broad range of spectroscopic signatures. This poses a challenge as conventional histopathology does not describe the heterogeneity in terms of metabolic states. The intrinsic fluorophores potentially being responsible for the distinct fluorescence emission spectrum include NADH/NAD(P)H at 460 nm and glutamate decarboxylase GAD or pyridoxamine-5-phosphate (PMP) at 390 nm. The characteristics of these fluorophores have been discussed in details previously (Butte et al., 2010). The emission characteristic of such fluorophores most likely is distinctly modulated by distinct tumor pathophysiology and metabolic states.

For example, LGG reported in this study were histopathologically sub-classified into oligoastrocytoma, oligodendroglioma and diffuse astrocytoma. TR-LIFS measurements conducted in these distinct types of LGG demonstrated variation in fluorescence signatures. We determined (Fig. 4A) that diffuse astrocytoma demonstrated longer τ_f at 390 nm when compared with both oligoastrocytoma and oligodendroglioma and this resulted in an increase of the overall lifetime values for LGG, when compared with those reported in our pilot study (Butte et al., 2010), in which only oligoastrocytoma and oligodendroglioma were investigated. When the oligoastrocytoma and oligodendroglioma ($\tau_{390} = 1.58 \pm 0.2$ ns) were grouped separately, their fluorescence characteristics followed a similar trend as those previously reported ($\tau_{390} = 1.45 \pm 0.4$ ns). This is clinically significant because oligodendroglioma tend to be more circumscribed, respond well to chemotherapy than astrocytoma and the patients have longer survival rates (Watanabe et al., 2002). On the other hand the low grade diffuse astrocytoma diffusely infiltrate the surrounding normal brain and have greater tendency to progress to a more malignant histological type, and are resistant to chemotherapy. Also, the low grade diffuse astrocytomas have a different genetic profile compared to oligodendroglioma, which may reflect the variation in the fluorescence signatures. It is also important to note that the fluorescence signature of diffuse astrocytoma closely resembled HGG, as diffuse astrocytoma

are more likely to rapidly transform to more malignant tumors such as anaplastic astrocytoma and glioblastoma. Thus a similar fluorescence signature may help in determining the prognosis of the treatment. If this diagnosis can be made during the excision then, autofluorescence may potentially be helpful in determining the course of therapy.

Similarly, when HGG samples were histopathologically sub-classified in glioblastoma multiforme, anaplastic oligodendroglioma and recurrent glioma with radiation necrosis, TR-LIFS characteristics were distinct for each group. It was observed (Fig. 4B) that anaplastic oligodendroglioma demonstrated longer τ_f at 390 nm when compared with glioblastoma multiforme and recurrent glioma and this also resulted in an increase of the overall lifetime values for HGG. Additionally, anaplastic oligodendroglioma samples demonstrated higher fluorescence emission intensity at 390 nm when compared to GBM. These factors resulted in lower classification accuracy of HGG. It is to be noted that the low grade oligodendroglioma samples have a shorter lifetime at a blue shifted wavelength of 390 nm compared with the high grade oligodendroglioma. Clinically, this indicates that it may be possible in the future to diagnose the progression of oligodendroglial tumors from being benign to malignant. Alternately, GBM was characterized by a shorter lifetime at 390 nm compared with normal tissues. This is significant as it enables TR-LIFS to characterize GBM from normal tissues using few selective wavelengths. Lastly, recurrent glioma with radiation necrosis did not have significant emission intensity at 440–460 nm of wavelength. This is an expected result as amount of viable cells in the necrotic tissue are fewer leading to absence or deficiency of NADH/NAD(P)H.

Taken together, these findings suggest that a large number of patients would need to be involved in determining the changes in TR-LIFS signal as a function of both biological diversity and heterogeneities in brain tumors both LGG and HGG. This underscores the need to elucidate fluorescence signatures within the HGG and LGG sub-sets as such signatures can potentially be related with patient prognosis.

(B) One of the major challenges in the validation of the new proposed technology (TR-LIFS) is correlation of the TR-LIFS point measurement with the pathology or biochemical characteristics of the biopsy tissue specimen acquired from the same site. This is due to a number of reasons. Firstly, the size of the optically interrogated volume (~ 1.2 mm surface diameter \times 250–400 μ m penetration depth) as defined by the fiber probe excitation-collection geometry and the UV light penetration depth, respectively, is typically smaller than the actual size of the biopsied tissue (~ 3 –4 mm³ depth). The orientation of the biopsy also cannot be determined making it hard to determine the exact tissue volume excited by the laser. Secondly, while numerous TR-LIFS measurements can be taken from a single patient, only a limited number of biopsies are obtained thus extensive validation of TR-LIFS measurements against local tissue pathology is limited. Studies to determine the intra-patient signal variability are therefore hard to achieve. Finally, due to high risk of damage to the functioning normal cortex, the spectroscopic features from normal cortex cannot be confirmed with biopsy. We are currently developing a new protocol to include patients undergoing surgical intervention for trauma and epilepsy in order to overcome this limitation.

(C) Maximizing the signal-to-noise ratio (SNR) for improved detection sensitivity and minimizing the time of data acquisition are important features of a TR-LIFS system capable of providing diagnostic information based on endogenous contrast and of operating in an intra-operative setting. The current experimental set-up (relative long data acquisition time of ~ 30 s) also imposed some challenges as related with the variable amount of blood in the field of measurement. This potentially results in the distortion of the fluorescence intensity and reduction of the signal-to-noise ratio (SNR). We noticed that the use of a spacer between the optical probe and tissue and presence of a slit in the spacer which enabled suction to remove the blood in the optical path during the experiments has minimized the fluorescence

signal re-absorption. This is demonstrated by a lower hemoglobin absorption “valley” at 415 nm in current study in contrast to our pilot study (Butte et al., 2010) where no such approach was used. Although the use of intensity ratio minimizes the absorptive effect of hemoglobin it does not entirely negate the effect on the intensity values. Correcting the spectral intensity for blood absorption will result in more accurate analysis. Maintaining the constant excitation-collection geometry via the spacer which stabilizes the probe on the brain tissue has also minimized the distortion of the fluorescence emission spectral shape.

A close analysis of spectroscopic parameters derived from both spectral and time domains demonstrated that a set of parameters combining spectro-temporal features are needed in order to accurately discriminate between distinct tissue types. By determining the optimal spectral bands for discrimination of pathologic vs. normal conditions, the TR-LIFS data acquisition can be reduced to a limited number of spectral bands. This is important as it will enable development of specialized TR-LIFS systems that collect fluorescence pulse transients at a limited number of wavelength bands as recently reported (Sun et al., 2008). In turn this will result in shorter data acquisition time (less than 1 s per point measurement), thus minimize photobleaching effects, virtually eliminating motion artifacts, and relaxing the need for continuous removal/suction of blood from the field of view.

Currently, a few optical techniques are being evaluated for their potential to aid the surgeon intra-operatively to completely excise the tumor tissue and for diagnosis. This includes steady-state autofluorescence combined with diffuse-reflectance spectra (Lin et al., 2005, 2001; Majumder et al., 2007; Toms et al., 2005) and fluorescence guided surgery using 5-aminolevulinic acid (Haj-Hosseini et al., 2010; Widhalm et al., 2010). The former technique that also uses 337 nm to induce tissue fluorescence was evaluated for its ability to discriminate between tumor core and tumor margin from normal human brain tissue (Lin et al., 2005, 2001; Majumder et al., 2007; Toms et al., 2005). The classification accuracy was reported as being approximately 96%, 80% and 97% respectively. While our findings related to the fluorescence spectral emission are in agreement with these previous studies, no extensive comparison can be made given that in present study the spectra were not corrected using reflectance spectroscopy and differences in experimental apparatus for spectral evaluation. For example, current results underscore that the fluorescence emission centered around 450–460 nm (attributed to NADH) plays an important role in distinct types of brain tissue discrimination. In addition, present study demonstrates that the fluorescence lifetime (ranging from ~ 1.2 ns to ~ 1.7 ns) corresponds to the protein bounded NADH (Jameson et al., 1989; Konig et al., 1997).

The second technique currently evaluated in clinical trials is based on exogenous fluorescence contrast due to 5-aminolevulinic acid (ALA) (Haj-Hosseini et al., 2010; Muller and Wilson, 2006; Widhalm et al., 2010). In this approach, the heme biosynthetic pathway is used to produce protoporphyrin IX (PpIX)—a photosensitizer for both tumor visualization and therapy. While this dual function is important and clinically relevant, one of the drawbacks of this technique is that 5-ALA has to be systemically administered before the procedure. The surgery needs to be performed in a limited time window. Secondly, during surgical procedures, there is vascular extravasation of fluorescent macromolecule, which may lead to loss of ability to visualize the tumor.

At our present stage of research, TR-LIFS does not compare with the existing standard of diagnosis using histopathology. However, our results suggest that this technique has the potential to delineate brain tumors from normal cortex to achieve improved tumor excision. The main goal of developing this technique is not to replace the existing gold standard of histopathology, but to provide a guide to the neurosurgeon during tumor resection. Based on the present results, acquiring additional data, in order to differentiate the subclasses of

tumors, would allow us to explore the potential of TR-LIFS technique further. Like with all the current techniques deployed in the operating room such as stereotactic navigation, intra-operative ultrasound, frozen section which provide guidance to surgeon regarding the extent of the tumor, it is task of the surgeon to interpret the results based on a full visual, tactile, imaging and special data. All the techniques mentioned above provide the surgeon with the structural information; TR-LIFS can be an additional technique which will enhance the ability of the surgeon to further evaluate the tissue by providing biochemical and metabolic information. The most important advantage of TR-LIFS is the speed at which it can provide the diagnosis, eliminating the requirement to repeat lengthy “frozen section.” The speed will also allow the surgeon to inspect multiple sites during the surgery thus decreasing the chances of residual tumor and ensuring more complete resection. Currently, the technique is used as a single point spectroscopy, but newer techniques are being developed by adapting fluorescence lifetime imaging to obtain a two dimensional image (Sun et al., 2008, 2009). This is anticipated to provide a more robust data and also provide a more useful diagnostic tool. In addition to brain tumors, TR-LIFS may have utility in detecting breast tumors, lung cancers, skin cancer, etc. Once clinically relevant information can be correlated with TR-LIFS features, TR-LIFS can be deployed clinically in number of ways, e.g. a point spectroscopy tool can be used as a smart biopsy probe inserted prior to tissue removal to reduce failure rates, intra-operatively a similar tool can compliment the frozen section based diagnostics. Using techniques such as raster scanning or detectors such as streak camera, intensified CCD (ICCD), it will be possible to resolve lifetime fluorescence from a larger area, and overlaying the information to the surgeon using operating microscope or heads-up-display (HUD), aiding in near-complete resection.

Conclusion

We have tested a prototype TR-LIFS system in the operating environment to study the fluorescence emission characteristics of low and high grade glioma tumors and normal brain tissue. Current results show that recording the intrinsic fluorescence of brain tumors and normal brain tissue intra-operatively has the potential to distinguish LGG from normal tissue with high accuracy and specificity. HGG demonstrated a high degree of heterogeneity, thus reducing the discrimination accuracy of these tumors as a broad category. The classification accuracy of TR-LIFS can be improved by obtaining more samples and using finer classification of brain tumors based on metabolic state and biochemical information. Further study of brain tumors with TR-LIFS will positively lead to more robust classification. In future studies, we plan to include additional classification criteria such as immune-histochemical analysis, further genetic sub-classification, and prognostic factors. We have demonstrated that TR-LIFS holds the potential to characterize distinct types of glioma tumors, to diagnose brain tumors intra-operatively and thus can be a valuable tool for aiding the surgeon in near complete resection of the brain tumors.

Conflict of interest statement

The authors declare that they have no conflict of interest.

Acknowledgments

This study was supported in part by the National Institutes of Health (Grant number: R42 CA117286) and the Whitaker Foundation.

The study conducted was approved by Cedars-Sinai Medical Center Institutional Review Board.

References

- Andersson-Engels, S., Johansson, J., Stenram, U., Svanberg, K., Svanberg, S., 1990. Time-resolved laser-induced fluorescence spectroscopy for enhanced demarcation of human atherosclerotic plaques. *J. Photochem. Photobiol. B* 4, 363–369.
- Baron, A.E., 1991. Misclassification among methods used for multiple group discrimination—the effects of distributional properties. *Stat. Med.* 10, 757–766.
- Bello, A.L., 1992. Misclassification among methods used for multiple group discrimination—the effects of distributional properties. *Stat. Med.* 11, 1623–1624.
- Berger, M.S., 1994. Malignant astrocytomas: surgical aspects. *Semin. Oncol.* 21, 172–185.
- Beychok, S., Tyuma, I., Benesch, R.E., Benesch, R., 1967. Optically active absorption bands of hemoglobin and its subunits. *J. Biol. Chem.* 242, 2460–2462.
- Bottiroli, G., Croce, A.C., Locatelli, D., Marchesini, R., Pignoli, E., Tomatis, S., Cuzzoni, C., Di Palma, S., Dalfante, M., Spinelli, P., 1995. Natural fluorescence of normal and neoplastic human colon: a comprehensive “ex vivo” study. *Lasers Surg. Med.* 16, 48–60.
- Bottiroli, G., Croce, A.C., Locatelli, D., Nano, R., Giombelli, E., Messina, A., Benericetti, E., 1998. Brain tissue autofluorescence: an aid for intraoperative delineation of tumor resection margins. *Cancer Detect. Prev.* 22, 330–339.
- Brandes, A.A., Tosoni, A., Franceschi, E., Reni, M., Gatta, G., Vecht, C., 2008. Glioblastoma in adults. *Crit. Rev. Oncol. Hematol.* 67, 139–152.
- Butte, P.V., Pikul, B.K., Hever, A., Yong, W.H., Black, K.L., Marcu, L., 2005. Diagnosis of meningioma by time-resolved fluorescence spectroscopy. *J. Biomed. Opt.* 10, 064026.
- Butte, P.V., Fang, Q., Jo, J.A., Yong, W.H., Pikul, B.K., Black, K.L., Marcu, L., 2010. Intra-operative delineation of primary brain tumors using time-resolved fluorescence spectroscopy. *J. Biomed. Opt.* 15.
- Byar, D.P., Green, S., Strike, T.A., Walker, M.D., 1983. Prognostic factors for malignant glioma. *Oncology of the nervous system. Martinus Nijhoff, Boston.* pp. 379–395.
- Chung, Y.G., Schwartz, J.A., Gardner, C.M., Sawaya, R.E., Jacques, S.L., 1997. Diagnostic potential of laser-induced autofluorescence emission in brain tissue. *J. Korean Med. Sci.* 12, 135–142.
- Croce, A.C., Fiorani, S., Locatelli, D., Nano, R., Ceroni, M., Tancioni, F., Giombelli, E., Benericetti, E., Bottiroli, G., 2003. Diagnostic potential of autofluorescence for an assisted intraoperative delineation of glioblastoma resection margins. *Photochem. Photobiol.* 77, 309–318.
- Cubeddu, R., Ramponi, R., Liu, W.Q., Docchio, F., 1989. Time-gated fluorescence spectroscopy of the tumor localizing fraction of HpD in the presence of cationic surfactant. *Photochem. Photobiol.* 50, 157–163.
- Cubeddu, R., Taroni, P., Valentini, G., Canti, G., 1992. Use of time-gated fluorescence imaging for diagnosis in biomedicine. *J. Photochem. Photobiol. B* 12, 109–113.
- Cubeddu, R., Pifferi, A., Taroni, P., Valentini, G., Canti, G., 1995. Tumor detection in mice by measurement of fluorescence decay time matrices. *Opt. Lett.* 20, 2553.
- Dickinson, R.B., Wehry, E.L., 1979. Time-resolved matrix-isolation fluorescence spectrometry of mixtures of polycyclic aromatic hydrocarbons. *Anal. Chem.* 51, 778–780.
- Ducray, F., Dutertre, G., Ricard, D., Gontier, E., Idbaih, A., Massard, C., 2010. Advances in adults' gliomas biology, imaging and treatment. *Bull. Cancer* 97, 17–36.
- Elson, D., Requejo-Isidro, J., Munro, I., Reavell, F., Siegel, J., Suhling, K., Tadrous, P., Banninger, R., Lanigan, P., McGinty, J., Talbot, C., Treanor, B., Webb, S., Sandison, A., Wallace, A., Davis, D., Lever, J., Neil, M., Phillips, D., Stamp, G., French, P., 2004. Time-domain fluorescence lifetime imaging applied to biological tissue. *Photochem. Photobiol. Sci.* 3, 795–801.
- Fang, Q., Papaioannou, T., Jo, J.A., Vaitha, K., Marcu, L., 2004. Time-domain laser-induced fluorescence spectroscopy apparatus for clinical diagnostics. *Rev. Sci. Instrum.* 75, 151–162.
- Fazekas, J.T., 1977. Treatment of grades I and II brain astrocytomas. The role of radiotherapy. *Int. J. Radiat. Oncol. Biol. Phys.* 2, 661–666.
- Haj-Hosseini, N., Richter, J., Andersson-Engels, S., Wardell, K., 2010. Optical touch pointer for fluorescence guided glioblastoma resection using 5-aminolevulinic acid. *Lasers Surg. Med.* 42, 9–14.
- Hartmann, C., Meyer, J., Balss, J., Capper, D., Mueller, W., Christians, A., Felsberg, J., Wolter, M., Mawrin, C., Wick, W., Weller, M., Herold-Mende, C., Unterberg, A., Jeuken, J.W., Wesseling, P., Reifenberger, G., von Deimling, A., 2009. Type and frequency of IDH1 and IDH2 mutations are related to astrocytic and oligodendroglial differentiation and age: a study of 1,010 diffuse gliomas. *Acta Neuropathol.* 118, 469–474.
- Jameson, D.M., Thomas, V., Zhou, D.M., 1989. Time-resolved fluorescence studies on NADH bound to mitochondrial malate dehydrogenase. *Biochim. Biophys. Acta* 994, 187–190.
- Jo, J.A., Fang, Q., Papaioannou, T., Marcu, L., 2004a. Fast model-free deconvolution of fluorescence decay for analysis of biological systems. *J. Biomed. Opt.* 9, 743–752.
- Jo, J.A., Fang, Q., Papaioannou, T., Qiao, J.H., Fishbein, M.C., Dorafshar, A., Reil, T., Baker, D., Freischlag, J., Marcu, L., 2004b. Novel methods of time-resolved fluorescence data analysis for in-vivo tissue characterization: application to atherosclerosis. *Conf. Proc. IEEE Eng. Med. Biol. Soc.* 2, 1372–1375.
- Jo, J.A., Fang, Q., Papaioannou, T., Qiao, J.H., Fishbein, M.C., Beseth, B., Dorafshar, A.H., Reil, T., Baker, D., Freischlag, J., Marcu, L., 2005. Application of the laguerre deconvolution method for time-resolved fluorescence spectroscopy to the characterization of atherosclerotic plaques. *Conf. Proc. IEEE Eng. Med. Biol. Soc.* 6, 6559–6562.
- Jo, J.A., Marcu, L., Fang, Q., Papaioannou, T., Qiao, J.H., Fishbein, M.C., Beseth, B., Dorafshar, A.H., Reil, T., Baker, D., Freischlag, J., 2007. New methods for time-resolved fluorescence spectroscopy data analysis based on the Laguerre expansion technique—applications in tissue diagnosis. *Methods Inf. Med.* 46, 206–211.
- Konig, K., Berns, M.W., Tromberg, B.J., 1997. Time-resolved and steady-state fluorescence measurements of beta-nicotinamide adenine dinucleotide-alcohol dehydrogenase complex during UVA exposure. *J. Photochem. Photobiol. B* 37, 91–95.

- Kriegeskorte, N., Simmons, W.K., Bellgowan, P.S., Baker, C.I., 2009. Circular analysis in systems neuroscience: the dangers of double dipping. *Nat. Neurosci.* 12, 535–540.
- Lakowicz, J.R., 2006. Principles of fluorescence spectroscopy, 3rd ed. Springer, New York.
- Lin, W.C., Toms, S.A., Johnson, M., Jansen, E.D., Mahadevan-Jansen, A., 2001. In vivo brain tumor demarcation using optical spectroscopy. *Photochem. Photobiol.* 73, 396–402.
- Lin, W.C., Mahadevan-Jansen, A., Johnson, M.D., Weil, R.J., Toms, S.A., 2005. In vivo optical spectroscopy detects radiation damage in brain tissue. *Neurosurgery* 57, 518–525 discussion 518–525.
- Louis, D.N., Ohgaki, H., Wiestler, O.D., Cavenee, W.K., Burger, P.C., Jouvet, A., Scheithauer, B.W., Kleihues, P., 2007. The 2007 WHO classification of tumours of the central nervous system. *Acta Neuropathol.* 114, 97–109.
- Majumder, S.K., Gebhart, S., Johnson, M.D., Thompson, R., Lin, W.C., Mahadevan-Jansen, A., 2007. A probability-based spectroscopic diagnostic algorithm for simultaneous discrimination of brain tumor and tumor margins from normal brain tissue. *Appl. Spectrosc.* 61, 548–557.
- Marcu, L., Fishbein, M.C., Maarek, J.M., Grundfest, W.S., 2001. Discrimination of human coronary artery atherosclerotic lipid-rich lesions by time-resolved laser-induced fluorescence spectroscopy. *Arterioscler. Thromb. Vasc. Biol.* 21, 1244–1250.
- Marcu, L., Jo, J.A., Butte, P.V., Yong, W.H., Pikul, B.K., Black, K.L., Thompson, R.C., 2004. Fluorescence lifetime spectroscopy of glioblastoma multiforme. *Photochem. Photobiol.* 80, 98–103.
- Muller, P.J., Wilson, B.C., 2006. Photodynamic therapy of brain tumors—a work in progress. *Lasers Surg. Med.* 38, 384–389.
- Nithipatikom, K., McGown, L.B., 1987. Five- and six-component determinations using phase-resolved fluorescence spectroscopy and synchronous excitation. *Appl. Spectrosc.* 41, 395–399.
- Papaioannou, T., Preyer, N., Fang, Q., Carnohan, M., Ross, R., Brightwell, A., Cottone, G., Jones, L., Marcu, L., 2004. Effects of fiber-optic probe design and probe-to-target distance on diffuse reflectance measurements of turbid media: an experimental and computational study at 337 nm. *Appl. Opt.* 43, 2846–2860.
- Poon, W.S., Schomacker, K.T., Deutsch, T.F., Martuza, R.L., 1992. Laser-induced fluorescence: experimental intraoperative delineation of tumor resection margins. *J. Neurosurg.* 76, 679–686.
- Rausch, J.R., Kelley, K., 2009. A comparison of linear and mixture models for discriminant analysis under nonnormality. *Behav. Res. Methods* 41, 85–98.
- Robins, H.I., Lassman, A.B., Khuntia, D., 2009. Therapeutic advances in malignant glioma: current status and future prospects. *Neuroimaging Clin. N. Am.* 19, 647–656.
- Rosato, N., Mei, G., Finazzi-Agro, A., Tancini, B., Borri-Voltattorni, C., 1989. Time-resolved extrinsic fluorescence of aromatic-L-amino-acid decarboxylase. *Biochim. Biophys. Acta* 996, 195–198.
- Sanai, N., Berger, M.S., 2008. Glioma extent of resection and its impact on patient outcome. *Neurosurgery* 62, 753–764 discussion 264–756.
- Siegel, J., Elson, D.S., Webb, S.E., Lee, K.C., Vlandas, A., Gambaruto, G.L., Leveque-Fort, S., Lever, M.J., Tadrous, P.J., Stamp, G.W., Wallace, A.L., Sandison, A., Watson, T.F., Alvarez, F., French, P.M., 2003. Studying biological tissue with fluorescence lifetime imaging: microscopy, endoscopy, and complex decay profiles. *Appl. Opt.* 42, 2995–3004.
- Smith, J.S., Chang, E.F., Lamborn, K.R., Chang, S.M., Prados, M.D., Cha, S., Tihan, T., Vandenberg, S., McDermott, M.W., Berger, M.S., 2008. Role of extent of resection in the long-term outcome of low-grade hemispheric gliomas. *J. Clin. Oncol.* 26, 1338–1345.
- Sud, D., Zhong, W., Beer, D.G., Mycek, M.A., 2006. Time-resolved optical imaging provides a molecular snapshot of altered metabolic function in living human cancer cell models. *Opt. Express* 14, 4412–4426.
- Sun, Y., Liu, R., Elson, D.S., Hollars, C.W., Jo, J.A., Park, J., Marcu, L., 2008. Simultaneous time- and wavelength-resolved fluorescence spectroscopy for near real-time tissue diagnosis. *Opt. Lett.* 33, 630–632.
- Sun, Y., Phipps, J., Elson, D.S., Stoy, H., Tinling, S., Meier, J., Poirier, B., Chuang, F.S., Farwell, D.G., Marcu, L., 2009. Fluorescence lifetime imaging microscopy: in vivo application to diagnosis of oral carcinoma. *Opt. Lett.* 34, 2081–2083.
- Svensson, T., Andersson-Engels, S., Einarsdottir, M., Svanberg, K., 2007. In vivo optical characterization of human prostate tissue using near-infrared time-resolved spectroscopy. *J. Biomed. Opt.* 12, 014022.
- Toms, S.A., Lin, W.C., Weil, R.J., Johnson, M.D., Jansen, E.D., Mahadevan-Jansen, A., 2005. Intraoperative optical spectroscopy identifies infiltrating glioma margins with high sensitivity. *Neurosurgery* 57, 382–391 discussion 382–391.
- Umesh, S., Tandon, A., Santosh, V., Anandh, B., Sampath, S., Chandramouli, B.A., Sastry Kolluri, V.R., 2009. Clinical and immunohistochemical prognostic factors in adult glioblastoma patients. *Clin. Neuropathol.* 28, 362–372.
- Vishwanath, K., Pogue, B., Mycek, M.A., 2002. Quantitative fluorescence lifetime spectroscopy in turbid media: comparison of theoretical, experimental and computational methods. *Phys. Med. Biol.* 47, 3387–3405.
- Wagnieres, G.A., Star, W.M., Wilson, B.C., 1998. In vivo fluorescence spectroscopy and imaging for oncological applications. *Photochem. Photobiol.* 68, 603–632.
- Watanabe, T., Nakamura, M., Kros, J.M., Burkhard, C., Yonekawa, Y., Kleihues, P., Ohgaki, H., 2002. Phenotype versus genotype correlation in oligodendrogliomas and low-grade diffuse astrocytomas. *Acta Neuropathol.* 103, 267–275.
- Widhalm, G., Wolfsberger, S., Minchev, G., Woehrer, A., Krssak, M., Czech, T., Prayer, D., Asenbaum, S., Hainfellner, J.A., Knosp, E., 2010. 5-Aminolevulinic acid is a promising marker for detection of anaplastic foci in diffusely infiltrating gliomas with nonsignificant contrast enhancement. *Cancer* 116, 1545–1552.
- Yan, H., Bigner, D.D., Velculescu, V., Parsons, D.W., 2009. Mutant metabolic enzymes are at the origin of gliomas. *Cancer Res.* 69, 9157–9159.
- Yaroslavsky, A.N., Schulze, P.C., Yaroslavsky, I.V., Schober, R., Ulrich, F., Schwarzaier, H.J., 2002. Optical properties of selected native and coagulated human brain tissues in vitro in the visible and near infrared spectral range. *Phys. Med. Biol.* 47, 2059–2073.
- Yong, W.H., Butte, P.V., Pikul, B.K., Jo, J.A., Fang, Q., Papaioannou, T., Black, K., Marcu, L., 2006. Distinction of brain tissue, low grade and high grade glioma with time-resolved fluorescence spectroscopy. *Front. Biosci.* 11, 1255–1263.